# **Journal Name**



# **ARTICLE TYPE**

Cite this: DOI: 10.1039/xxxxxxxxxx

# Effect of Surface Ligands on Gold Nanocatalysts for CO<sub>2</sub> Reduction

Hongyu Shang $^{a,\P}$ , Spencer K. Wallentine $^{a,\P}$ , Daniel M. Hofmann, $^b$  Quansong Zhu $^a$ , Catherine J. Murphy $^b$  and L. Robert Baker $^{a*}$ 

Received Date Accepted Date

DOI: 10.1039/xxxxxxxxxx

www.rsc.org/journalname

Nanoparticle catalysts display optimal mass activity due to their high surface to volume ratio and tunable size and structure. However, control of nanoparticle size requires the presence of surface ligands, which significantly influence catalytic performance. In this work, we investigate the effect of dodecanethiol on the activity, selectivity, and stability of Au nanoparticles for electrochemical carbon dioxide reduction (CO<sub>2</sub>R). Results show that dodecanethiol on Au nanoparticles significantly enhances selectivity and stability with minimal loss in activity by acting as a  ${\rm CO_2}$ -permeable membrane, which blocks the deposition of metal ions that are otherwise responsible for rapid deactivation. Although dodecanethiol occupies 90% or more of the electrochemical active surface area, it has a negligible effect on the partial current density to CO, indicating that it specifically does not block the active sites responsible for CO<sub>2</sub>R. Further, by preventing trace ion deposition, dodecanethiol stabilizes CO production on Au nanoparticles under conditions where CO<sub>2</sub>R selectivity on polycrystalline Au rapidly decays to zero. Comparison with other surface ligands and nanoparticles shows that this effect is specific to both the chemical identity and the surface structure of the dodecanethiol monolayer. To demonstrate the potential of this catalyst, CO<sub>2</sub>R was performed in electrolyte prepared from ambient river water, and dodecanethiol-capped Au nanoparticles produce more than 100 times higher CO yield compared to clean polycrystalline Au at identical potential and similar current.

## 1 Introduction

Nanoparticle catalysis benefits from inherently high surface to mass ratios and controllable surface structure, <sup>1–3</sup> size, <sup>4,5</sup> shape, <sup>3,6,7</sup> and composition <sup>4,8</sup>, which offer the ability to tune the activity and selectivity of heterogeneous catalytic systems. <sup>9</sup> These properties are often controlled using small molecules or polymers, called capping agents, which coordinate to surface atoms during synthesis. <sup>10</sup> Despite providing a high degree of synthetic control, from a catalysis perspective, organic capping agents are usually undesired because this inert layer occupies the majority of potentially active surface sites on the nanoparticle catalyst. Consequently, effort is usually made to remove the capping agent from a nanoparticle catalyst prior to use. <sup>10,11</sup> However, there have been a number of studies which show that surface ligands can actually enhance selectivity <sup>12–17</sup> and even activity. <sup>18–21</sup> For exam-

Many heterogeneous reactions, like carbon dioxide reduction (CO<sub>2</sub>R), have a strong surface structure dependence.  $^{26-28}$  Both theoretical and experimental studies have shown that CO<sub>2</sub>R on Au primarily occurs at undercoordinated sites (i.e. coordination number  $\leq 7)$ .  $^{29-33}$  Single crystal studies on Au show that these sites are at least 20-fold more active for CO<sub>2</sub>R than the more coordinated terrace sites.  $^{29}$  In that same study underpotential deposition also showed that these low-coordination sites are the first to poison by electrodeposition of divalent cations. It is well documented that electrodeposition of metal cations on an electrode surface during CO<sub>2</sub>R leads to catalyst deactivation,  $^{34-36}$  making electrolyte purity a difficult but important parameter to control. Considering the cost associated with water purification, this is an often overlooked challenge that is intimately related to the economic viability of aqueous CO<sub>2</sub> conversion and utilization.  $^{37,38}$ 

In this work we investigate the influence of an organic passivation layer on the catalytic performance of small Au nanoparticles, having a 2 nm diameter, for electrochemical CO<sub>2</sub>R. We

ple, capping agents have been shown to promote catalyst performance through selective site blocking, <sup>22,23</sup> ligand substrate interactions, <sup>24,25</sup> or by providing prolonged stability. <sup>21</sup> These surface ligands can provide a homogeneous type handle to control heterogeneous catalysis.

<sup>&</sup>lt;sup>a</sup> The Ohio State University, Columbus, Ohio, USA. E-mail: baker.2364@osu.edu

<sup>&</sup>lt;sup>b</sup> University of Illinois at Urbana-Champaign, Urbana, Illinois, USA.

<sup>†</sup> Electronic Supplementary Information (ESI) available: [details of any supplementary information available should be included here]. See DOI: 00.0000/00000000. \$ Additional footnotes to the title and authors can be included e.g. 'Present address:' or 'These authors contributed equally to this work' as above using the symbols: \$, \$, and ¶. Please place the appropriate symbol next to the author's name and include a \footnotetext entry in the the correct place in the list.

compare the activity, selectivity, and deactivation of the following systems: 1) as prepared Au nanoparticles containing a layer of 1-dodecanethiol (DDT-Au), 2) Au nanoparticles following removal of the dodecanethiol ligand by UV/ozone cleaning (UVO-Au), 3) Au nanoparticles of identical size prepared with a layer of triphenylphosphine in place of dodecanethiol (PPh<sub>3</sub>-Au), 4) CuAu bimetallic nanoparticles of identical size prepared with a layer of dodecanethiol (DDT-CuAu), and 5) polycrystalline Au (PC-Au) with and without a self-assembled monolayer (SAM) of dodecanethiol. Unless otherwise noted, measurements were performed in CO<sub>2</sub>-saturated 0.1 M sodium bicarbonate (pH=6.8) at -1.1 V vs RHE. To determine the effects of surface poisoning by electrodeposition of trace divalent metal ions, CO2R kinetics were compared in the presence and absence of 3.4  $\mu$ M EDTA, which has been previously reported to prevent electroplating of divalent metal ions by strong chelation.<sup>39</sup>

We find that while dodecanethiol reductively desorbs from polycrystalline Au surfaces before the onset of CO<sub>2</sub>R, a stable population of dodecanethiol exists on the Au nanoparticle surface under CO<sub>2</sub>R reaction conditions at potentials as low as -1.1 V vs RHE. Although the presence of dodecanethiol decreases the electrochemical active surface area of the Au nanoparticles, it has only a small effect on CO<sub>2</sub>R current. This is confirmed by similar initial partial currents of CO production on DDT-Au, PC-Au and UVO-Au. These findings suggest that while the dodecanethiol layer passivates the majority of the Au terrace sites, it specifically does not block the edge and/or corner sites, which are primarily responsible for CO<sub>2</sub>R. Additionally, not only does the capping layer not limit CO2R activity, we find that it greatly increases the catalyst stability by preventing the deposition of trace metal cations. In essence, this capping layer, which is permeable to CO2 is almost completely impermeable to divalent metal cations, providing enhanced stability with almost no decrease in catalytic activity. Finally, we show that this protecting effect is specific to both the chemical identity and the structure of the organic capping layer.

Specifically, we observe that on  $PPh_3$ -Au Faradaic selectivity to CO decays rapidly, indicating that, unlike DDT,  $PPh_3$  does not block ion deposition. Likewise, we find that DDT-capped CuAu nanoparticles also do not resist deactivation. On DDT-CuAu we observe reduced selectivity to CO and increased  $H_2$  evolution, consistent with the effects of Cu addition. However, focusing on catalyst stability, we find that the Faradaic efficiency to CO on DDT-CuAu rapidly decays, similar to PC-Au and  $PPh_3$ -Au. We attribute to this to the reduced order and lower heat of adsorption of DDT on bimetallic CuAu nanoparticles compared to pure Au as characterized by vibrational sum frequency generation (SFG) spectroscopy.

# 2 Results and Discussion

Nanoparticles were drop-casted onto a glassy carbon electrode prior to measuring  $CO_2R$  kinetics in an electrochemical H-cell (see supporting information section 1 for additional experimental details). The nanoparticle mass loading was carefully selected to yield the same electrochemical active surface area (ECSA) for clean Au nanoparticles following ligand removal (i.e. UVO-Au) as for a clean PC-Au electrode. The capping agent was removed

Sample	$I_{CO}(mA)$	ECSA (cm <sup>2</sup> )	$TOF(\frac{molecules}{site*s})$
DDT-Au	0.81	0.15	14
PC-Au	0.80	1.2	1.8
UVO-Au	1.14	1.2	2.4

**Table 1** Partial CO current ( $I_{CO}$ ), electrochemical active surface area (ECSA), and turn over frequency (TOF) of DDT-Au, PC-Au, and UVO-Au catalysts.

using UV generated ozone and washed with milli-Q water. 40 This process was sufficient to completely remove the dodecanethiol capping agent as confirmed by XPS measurements, which show complete elimination of the S 2p signal after cleaning (see Figure S2 in supporting information section 1). TEM images of UVO-Au immediately following DDT removal by UV-ozone shows that removal of the surface ligand results in nanoparticle aggregation, and we find that it is impossible to stabilize the nanoparticle morphology in the absence of the surface ligand. This makes it difficult to quantify the exact fraction of the nanoparticle surface occupied by the DDT ligand because comparing ECSA before and after UV-ozone cleaning shows an increase in surface area resulting from ligand removal, but this is partially offset by a loss of geometric surface area caused by nanoparticle aggregation. Consequently, the ratio of ECSA measured before and after ligand removal represents a lower limit to the fraction of the Au nanoparticle occupied by the surface, and an even higher surface area would be observed after ligand removal if aggregation did not occur. Table 1 compares the ECSA measured by cyclic voltammetry, the partial current to CO measured by head space sampling, and the corresponding turnover frequency (TOF) using ECSA as an estimate for active site density. This comparison is provided for DDT-Au, PC-Au, and UVO-Au samples. As shown, the UVO-Au has a similar ECSA as the PC-Au, which is by design based on the mass loading of the drop cast samples. However, comparing the ECSA between DDT-Au and UVO-Au shows that the ECSA is 8-fold higher for UVO-Au than DDT-Au, indicating that the dodecanethiol capping agent occupies, as a minimum, at least 88% of the Au surface sites (for details of the ECSA measurements, see supporting information section 2). This value represents the effective rather than absolute surface coverage and is defined by accessibility of redox species to the particle surface, compared to the absolute coverage, which is defined by the ratio between the number of Au surface atoms to the number of DDT molecules. Analysis of the S:Au atomic ratio measured by XPS allows us to additionally estimate the absolute surface coverage for DDT assuming a truncated polyhedron with a 1 nm radius as described in the supporting information section 3. This analysis indicates that the absolute coverage of DDT on Au is  $\sim$ 60%, and this value is in close agreement with previous reports by Hostetler et al. 41 Comparison of the effective and absolute coverage indicates that closely spaced DDT molecules on a Au surface are sufficient to block access of solvated redox species to the electrode even if every Au site is not occupied and provides insight into mass transport through the cybotactic region as discussed further below.

Despite having only a small fraction of the total accessible

ECSA, we find that the  $CO_2R$  activity of DDT-Au is nearly identical to a clean PC-Au surface as measured by the partial current to CO. Normalizing the CO partial current to the ECSA, it is possible to estimate the TOF assuming an active site density on Au of approximately  $1.2\times10^{15}$  sites/cm² (see supporting information section 4). This calculation provides a reasonable estimate of the average TOF of all exposed sites. The calculated TOF for DDT-Au is the highest (TOF=14), where the exposed sites are found to be approximately 8-fold more active than the average activity of PC-Au (TOF=1.8) and approximately 6-fold more active than the ensemble of sites present on UVO-Au (TOF=2.4). These values represent initial kinetics during the first 20 min of reaction and are normalized to ECSA measurements of fresh DDT-Au, PC-Au, and UVO-Au. Below we consider the possibility that both reaction rate and ECSA may evolve in time during the reaction.

Particularly we note that thiols on Au have been reported to electrochemically desorb at reducing potentials. Consequently, we carefully consider how the dodecanethiol surface ligand coverage and associated ECSA is changing in time during CO<sub>2</sub>R reaction conditions. Using XPS, the ratio of S 2p and Au 4f XPS shows how the ligand coverage changes with time. Table S2 in section 5 of the supporting information shows results for as-prepared DDT-Au nanoparticles and DDT-Au following 1 and 2 h reaction time. During the first 1 h of reaction time the S:Au ratio decreases from 0.33 to 0.11 indicating that two thirds of dodecanethiol desorbs. However, after 2 h the S:Au ratio only drops slightly to 0.07, indicating that the remaining DDT is largely stable on the surface during extended reaction times. Post reaction TEM confirms that the size distribution of DDT-Au doesn't change after 2 h of reaction time (see Figure S6 in the supporting information section 5) providing further evidence that a sufficient fraction of dodecanethiol is stable on the nanoparticle surface during CO<sub>2</sub>R as required to stabilize the small nanoparticle size. In contrast, measurements performed on PC-Au functionalized with dodecanethiol (DDT-PC-Au), shows that on planar Au the dodecanethiol surface ligand is completely removed within 1 h of reaction time. This indicates that while dodecanethiol is not electrochemically stable at reducing potentials on planar Au, its stability is enhanced on small nanoparticles for at least 2 hours, after which we see a slow loss in activity, presumably due to gradual loss of the capping agent (see Figure S8 supporting information section 5).

To further understand this, we also measure cyclic voltammograms of DDT-Au and compare this to DDT-PC-Au. These data are presented in Figure S7 in the supporting information section 5. To summarize, on a planar dodecanethiol functionalized PC-Au electrode, we observe a redox wave associated with the reductive desorption and oxidative re-adsorption of dodecanethiol from the Au electrode. Although the reduction peak of this wave overlaps with  $\rm H_2$  evolution and  $\rm CO_2$  reduction, the oxidation peak associated with re-adsorption is clearly visible, and these findings are consistent with previous reports of CV cycling of SAMs on Au electrodes.  $^{42,43}$  In contrast, we find that the same redox feature is notably absent in the CV curve for DDT-Au, even though vibrational spectroscopy and XPS both confirm the presence of dodecanethiol on the nanoparticle surface. This indicates that the reductive desorption of dodecanethiol on DDT-Au nanoparticles is shifted to

more negative potentials, and this is a result of the increased heat of adsorption of dodecanethiol on a small nanoparticle compared to bulk Au. For example, a study by Tsai et al. 44 showed that for Au nanoparticles, capped with 11-mercaptodecanoic acid, and ranging in size from 60 to 20 nm, the heat of adsorption of the thiol increases with decreasing nanoparticle size from 100 to 108 kJ/mol. In this study we use much smaller nanoparticles of only 2 nm diameter, where the heat of adsorption is expected to be even stronger. While the actual value for heat of adsorption for dodecanethiol on ultrasmall nanoparticles is beyond the scope of the present paper, at this stage we confirm that a population of the dodecanethiol is stable on the DDT-Au nanoparticle surface under the CO<sub>2</sub>R reaction conditions studied here. The persistence of this capping agent is further verified by its ability to effectively block electrodeposition of metal ions on the DDT-Au nanoparticle surface as discussed below.

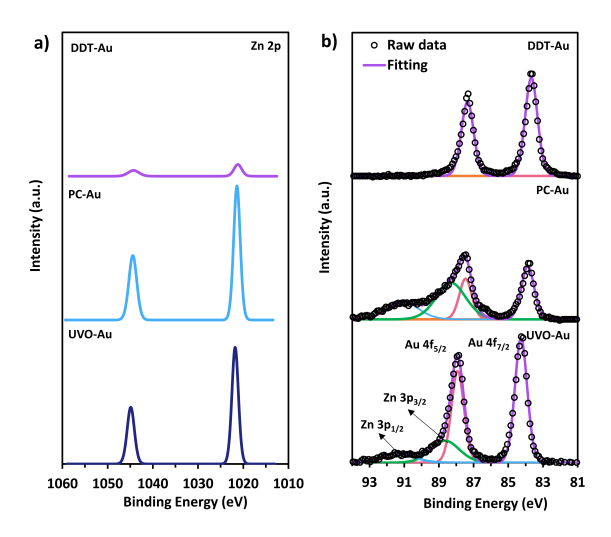


**Fig.** 1 XPS of (a) Zn 2p (b) Au 4f on DDT-Au, PC-Au and UVO-Au following electrolysis at -1.1 V vs RHE in 0.1 M sodium bicarbonate electrolyte containing 10  $\mu\text{M}$  of ZnCl $_2$ . Peak integration shows that the Zn:Au atomic ratio is 0.51, 8.32, and 3.08 on DDT-Au, PC-Au, and UVO-Au, respectively. The PC-Au and UVO-Au show additional peaks due to the overlap of the Au 4f $_{5/2}$  peak with the Zn 3p edge.  $^{45}$ 

To investigate the effect of the dodecanethiol SAM on the electrodeposition of metal cations, we prepared an electrolyte solution of 0.1 M sodium bicarbonate to which we added 10  $\mu M$ of ZnCl<sub>2</sub>. Concentrated Zn<sup>2+</sup> was used because Zn<sup>2+</sup> is a common contaminant in electrolyte solutions that is known to poison CO<sub>2</sub>R catalysts by electrodeposition during reaction, and because it is difficult to quantify the trace amount of ions in a deactivated sample by XPS. 39 Using this intentionally contaminated electrolyte, the catalysts were exposed to CO<sub>2</sub>R reaction conditions at an applied potential of -1.1 V vs RHE for 40 min, and then analyzed for the deposition of Zn using XPS. Results of the post-electrolysis XPS measurements are given in Figure 1. Both the PC-Au and UVO-Au samples show large amounts of Zn, having a Zn:Au atomic ratio of 8.32 and 3.08, respectively, following electrolysis. By comparison, relatively little Zn is found to deposit on the DDT-Au catalyst following identical treatment, which has a Zn:Au ratio of only 0.51. We note that 10  $\mu$ M ZnCl<sub>2</sub> represents much higher than normal impurity concentration, but this serves to illustrate the effect of dodecanethiol to limit electroplating on Au during  $CO_2R$ . Similar results are also observed for the electrodeposition of  $Cu^{2+}$  (see supporting information section 6). These results show the ability of the dodecanethiol capping layer to effectively prevent the approach and deposition of solvated  $Zn^{2+}$  ions onto the Au surface. This effect is fortuitous given the observation that this same surface passivation layer does little to block the accessibility of  $CO_2$  to Au sites which are active for  $CO_7R$ .

Given the ability of the capping layer to selectively block metal ion deposition during active CO<sub>2</sub>R, we investigated the kinetics of the same three catalysts described above in electrolyte containing only native ion contamination (i.e. no metal salts were intentionally introduced to the system). In these experiments, 18 M $\Omega$ water (Millipore) was used to prepare 0.1 M sodium bicarbonate electrolyte Sigma-Aldrich, >99.5%). Aside from using ultrapurified water and acid-cleaned glassware, no further steps were used to remove metal ion contamination. To illustrate the effects of surface poisoning by electrodeposition of trace divalent metal ions, CO2R kinetics were compared in the presence and absence of 3.4 µM EDTA, which has been previously reported to prevent electroplating of metal ions by strong chelation. <sup>39</sup> Figure 2 shows the results of these experiments for DDT-Au (a-c), PC-Au (d-f), and UVO-Au (g-i). In these experiments, CO<sub>2</sub>R reaction kinetics are determined by head space sampling every 20 min during the course of a 2 h reaction. <sup>1</sup>H-Nuclear Magnetic Resonance (NMR) analysis of the post-reaction electrolyte confirmed that no other products besides CO and H2 are produced, consistent with other reports of  $CO_2R$  on Au.  $^{46-48}$ 

As shown, PC-Au initially produces CO with 45% Faradaic selectivity. However, within approximately 100 min of reaction time, the Faradaic selectivity to CO decreases to nearly zero and only the  $\rm H_2$  evolution reaction remains active. This rapid deactivation is partially a result of metal ion contamination as evidenced by the comparison of this catalyst with and without the addition of 3.4  $\mu$ M EDTA to the electrolyte. In the presence of EDTA, which strongly chelates any trace transition metal ions, we find that the  $\rm CO_2R$  activity decays much more slowly. The initial Faradaic efficiency to CO during the first 20 min of reaction is also improved, presumably by preventing fast ion deposition during the initial several minutes of reaction, which occurs in the absence of EDTA.

In contrast, DDT-Au is completely resistant to deactivation by metal ion contamination. This can be seen by the constant Faradic selectivity during the course of the reaction as well as the nearly identical performance of this catalyst in the presence and absence of EDTA. Both these observations are consistent with the ability of dodecanethiol to block electrodeposition of metal ions at catalytic active sites on the Au surface as shown in Figure 1 above.

Lastly, UVO-Au is initially the most selective catalyst for  $CO_2R$ , having a Faradaic selectivity of approximately 60%. This catalyst is also more active than PC-Au despite having a similar ECSA. Comparing the Au 4f XPS spectra of DDT-Au before and after ligand removal by UV-ozone treatment shows a shift in the spectrum consistent with oxidation of the Au nanoparticles (see Figure S2

of the supporting information section 1). It has been reported that oxide-derived Au is highly active for  ${\rm CO_2}$  conversion to  ${\rm CO,}^{49,50}$  and we expect this effect as well as ligand removal both contribute to the increase in activity upon cleaning. Although initially active, this catalyst is prone to deactivation and CO production drops from 60% to 30% Faradaic selectivity during the course of the 2 h reaction. Although the stability of the UVO-Au catalyst is improved in the presence of EDTA, some deactivation is still observed. We attribute this deactivation, which occurs even in the presence of EDTA, to gradual reduction and time-dependent evolution of the surface structure for this oxide-derived Au catalyst during the course of the 2 h reaction.  $^{49}$ 

While the DDT-Au is more resistant to deactivation from ion deposition, it remains unclear whether this is a result of the ligand stabilized geometry, or a property of the ligand itself. This question is not trivial to answer because the ligand coverage and morphological stability are inherently coupled. To gain additional understanding about the influence of chemical identity and packing structure of the dodecanethiol capping agent on CO<sub>2</sub>R performance we prepared two additional samples: Au nanoparticles of similar size but with a triphenylphosphine rather than dodecanethiol surface layer (PPh3-Au) and CuAu bimetallic nanoparticles with a dodecanethiol surface layer (DDT-CuAu) also having the same 2 nm diameter. Although dodecanethiol forms a highly ordered SAM on a pure Au surface, addition of Cu atoms results in a significant decrease in the packing order. This can be observed in the vibrational SFG spectrum, where the relative intensity of the CH3 and CH2 stretches reflects the degree of packing order.  $^{51}$  Vibrational SFG spectra of a dodecanethiol SAM on PC-Au, DDT-Au, and DDT-CuAu are provided in the supporting information section 7. These spectra confirm that while dodecanethiol forms a well-ordered monolayer on planar PC-Au, and only a small density of gauche defects are observed on DDT-Au, the degree of disorder increases significantly on CuAu bimetallic nanoparticles. This means that the comparison of DDT-Au with PPh<sub>3</sub>-Au allows us to observe the effect of chemical identity, and the comparison with DDT-CuAu allows us to observe the effect of dodecanethiol packing order on the resulting CO2R reaction kinetics.

A summary of results for all catalysts tested here is provided in Figure 3. Solid bars show the initial CO current measured during the first 20 min of reaction, and dash bars show the CO current following 2 h of reaction time. The difference between the solid and dash bars indicate the effects of catalyst deactivation. To illustrate this more clearly, part f shows the relative CO<sub>2</sub>R activity following 2 h of reaction normalized to the initial rate, where a value of unity reflects no deactivation, and a value of zero reflects complete deactivation. We find that the PPh<sub>3</sub>-Au catalyst deactivates by approximately 85% during the experiment, indicating that triphenylphosphine is unable to protect the Au nanoparticle catalyst in the same manner as dodecanethiol. Similar to PPh<sub>3</sub>-Au, we find that DDT-CuAu also deactivates by approximately 55% over the course of the reaction.

As discussed above, it is not possible to perfectly disentangle the role of the DDT ligand and nanoparticle size in preventing ion deposition because ligand removal inherently alters the size

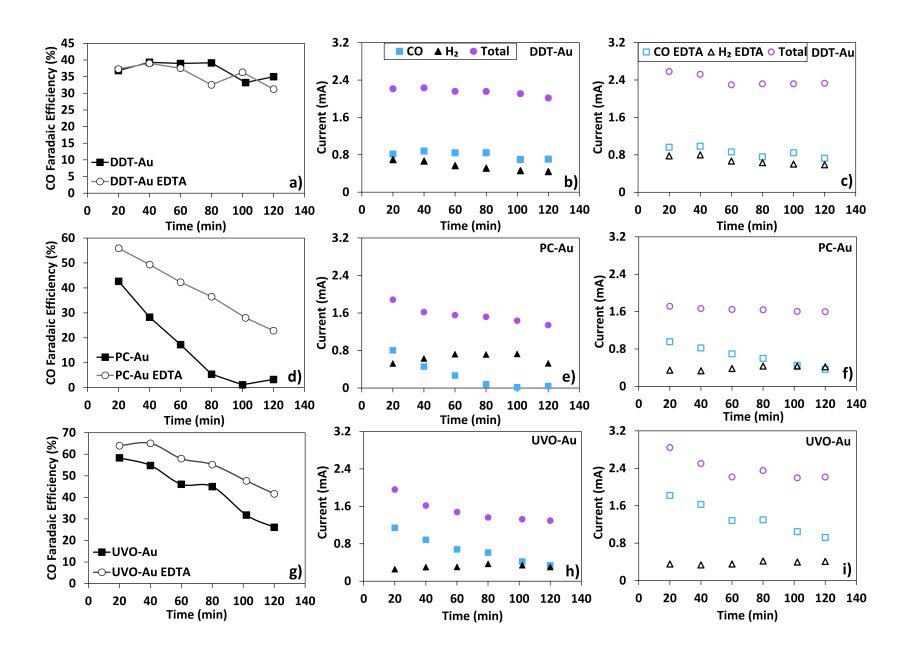


Fig. 2 Faradaic efficiency to CO and partial current of each product for DDT-Au (a b, and c), PC-Au (d, e and f). UVO-Au (g, h and i). Results are compared for 0.1 M sodium bicarbonate electrolyte with and without 3.4  $\mu$ M EDTA.

distribution. However, both of these control experiments indicate that the ligand itself rather than the particle morphology is responsible for the observed resistance to deactivation. In both cases, particles of nearly identical size show significant deactivation suggesting that DDT ligand binding and structure, which is unique to DDT-Au compared to either PPh3-Au or DDT-CuAu protects the catalytic particle from trace metal ion deposition. Further support for this conclusion can be found in the literature, where it was shown by single crystal studies that underpotential ion deposition on Au electrodes occurs preferentially at undercoordinated sites. <sup>29,36</sup> Because ultrasmall nanoparticles will have an increased density of low coordination sites as well as a higher surface energy, we believe it is unlikely resistance to ion deposition is related to the small particle size and instead conclude that the surface ligand is primarily responsible for the observed resistance to deactivation.

As shown in Figure 3e the total CO<sub>2</sub>R activity of the CuAu bimetallic catalyst is low compared to pure Au. This is because the addition of Cu results in decreased selectivity for CO and an increase in H<sub>2</sub> evolution (see supporting information section 8). These observations are consistent with previous reports, which show that very small Cu particles are also less selective for CO<sub>2</sub>R compared to larger Cu nanoparticles or bulk Cu catalysts. 52 Unlike pure Au, DDT-CuAu also produces HCOO- at 2% Faradic efficiency (see supporting information section 9). This is consistent with reports of CO<sub>2</sub>R on larger (8 nm) Cu-Au bimetallic particles, which also show small selectivity to HCOO-.48 However, focusing on the catalyst stability rather than overall activity, we find that the disordered structure of dodecanethiol on DDT-CuAu is less effective at preventing deactivation compared to DDT-Au. We attribute this to the combined effect of reduced order of DDT on bimetallic CuAu nanoparticles compared to pure Au as characterized by SFG spectroscopy as well as the weaker heat of adsorption

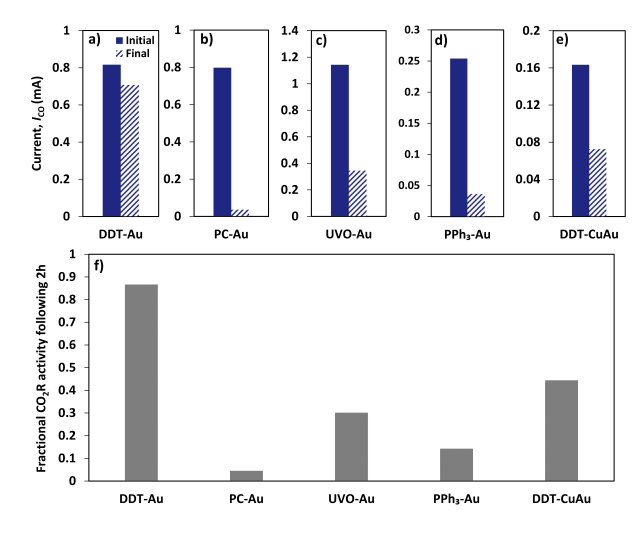


Fig. 3 Partial CO current for a) DDT-Au b) PC-Au c) UVO-Au d) PPh<sub>3</sub>-Au e) DDT-CuAu f) Catalyst deactivation plotted as relative  $CO_2R$  activity following 2 h of electrolysis at -1.1 v vs RHE for each sample.

of DDT on Cu compared to Au resulting in decreased catalyst stability. Of all the catalyst studied, only the DDT-Au sample resists significant deactivation, having approximately 90% of its initial activity following 2 h of reaction. These results indicate that both the chemical identity and packing order of the surface passivation layer contribute to the ability of dodecanethiol to protect the Au nanoparticles from deactivation.

To demonstrate the ability of the dodecanethiol capping agent to prevent catalyst deactivation and preserve  $CO_2R$  selectivity under non-ideal reaction conditions, we have performed kinetic measurements using electrolyte prepared with water obtained directly from the Olentangy River in Columbus, Ohio, USA. No purification except for particle filtration was performed. For refer-

ence, elemental analysis of this water is provided in the supporting information section 10.53 This ambient water was used to prepare a 0.1 M sodium bicarbonate electrolyte, which was purged with CO2 prior to electrolysis at -1.1 V vs RHE. Figure 4 shows the results of CO<sub>2</sub>R performed using DDT-Au and PC-Au in this electrolyte. Above we showed that DDT-Au displays enhanced selectivity and stability compared to PC-Au even in electrolyte prepared using ultra-purified water, and a similar but much greater effect is observed in this native system. As shown in Figure 4, the absolute current is nearly identical between these two catalysts, but CO<sub>2</sub>R activity to CO is more than 100 times greater on DDT-Au compared to PC-Au. Full kinetic plots showing the partial current to CO and H2 are provided in Figure S12 of the supporting information section 10. Not surprisingly, we observe that under these harsh conditions, DDT-Au shows signs of deactivation. However, we note that even following 2 h of electrolysis a steady production of CO is still observed, highlighting the usefulness of this system to operate under realistic conditions, not requiring tedious or expensive ultra-purification of reagents.

Au is one of the most selective known catalysts for conversion of CO2 to CO. While Au is highly selective, it is also precious, which motivates improved efforts to reduce consumption and increase catalyst lifetime. Both these goals are effectively addressed through the use of ultrasmall DDT-Au nanoparticles as described here. First, the use of ultrasmall particles decreases Au consumption by maximizing catalyst dispersion compared to larger Au nanoparticles or polycrystalline films. Second, these ultrasmall particles are stabilized by the DDT surface ligand, which is earth-abundant and cheap compared to Au. Not only does DDT serve to stabilize the ultrasmall particle size, but as shown here, it effectively prevents deactivation of active Au surface sites by electrodeposition of trace metal ions. Accordingly, DDT-Au provides optimal use of Au as an electrocatalyst for CO2 conversion by simultaneously maximizing dispersion while also significantly enhancing catalyst lifetime.

To consider the mechanism by which ligand-stabilized DDT-Au nanoparticles resist deactivation, we note that small nanoparticles have a high density of undercoordinated Au sites, which are known to be active for CO<sub>2</sub>R. <sup>29–33</sup> While it is possible that these active sites are also inherently more resistant to deactivation, we believe that this is unlikely for two reasons: First, we observe that EDTA serves to slow the selectivity loss for PC-Au and UVO-Au suggesting that ion deposition is one of the primary contributors to deactivation. Second, ions preferentially deposit at undercoordinated sites during underpotential deposition, <sup>29</sup> so one would expect that these active sites to be especially prone to poisoning by metal ions. To describe the selective nature of the dodecanethiol protecting layer, which is able to prevent deposition of metal ions, while allowing the approach of CO<sub>2</sub> to Au active sites, we consider that the Au nanoparticles employed here can be described as multi-faceted polyhedrons as shown in the High-Angle Annular Dark-Field Scanning Transmission Electron Microscope (HAADF-STEM) of Figure 5a. Additionally, we refer to the scale drawing in Figure 5b. We note that dodecanethiol forms a highly ordered SAM on Au terraces, 54 and we expect a large fraction of DDT to reside on the terraces. This is confirmed by vibrational

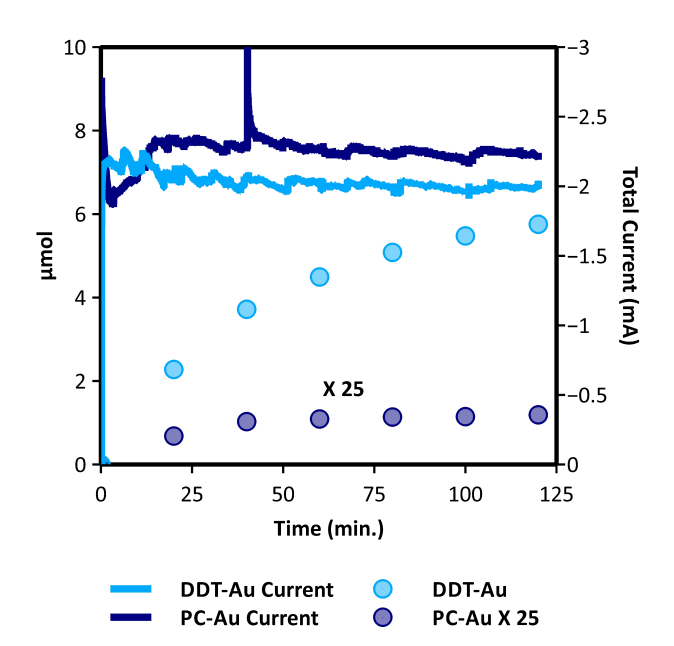


Fig. 4 Results of  $CO_2R$  on DDT-Au and PC-Au catalysts in  $CO_2$ -saturated 0.1 M NaHCO $_3$  electrolyte prepared from ambient river water with no purification except particle filtration. The plot shows the time dependent yield of CO and the total current. For comparison the CO yield from PC-Au is multiplied by 25.

SFG spectroscopy, which shows the presence of the SAM and indicates by the relative intensity of the  ${\rm CH_2}$  and  ${\rm CH_3}$  stretches, a high degree of order in the packing structure (see supporting information section 7). However on small nanoparticles, surface ligands will minimize steric forces by striving to maintain a constant volume fraction in the cybotactic region. Although dodecanethiol will be unable to tightly pack across the edge between adjacent terraces, a constant volume fraction can be maintained by the formation of gauche defects. This is confirmed by comparing the SFG spectra of dodecanethiol on DDT-Au and PC-Au, which shows an increase in gauche defects on DDT-Au compared to PC-Au, and we expect these gauche defects are primarily located near the edge sites. This is depicted in the scaled schematic in Figure 5b.

Based on the radius of a hydrated Zn<sup>2+</sup> (or similar divalent transition metal ions), this solvation complex would be unable to approach either a terrace or an edge site given the density of the DDT monolayer. Although we have shown that the dodecanethiol coverage evolves during reaction, still we observe almost no catalyst deactivation for reaction times up to 2 h. These results suggest that there is a critical surface coverage that is necessary to effectively block deposition of divalent ions. This may be related to the ability of gauche defects to increase the volume fraction of dodecanethiol surface ligands, enabling ion blocking even as the dodecanethiol coverage decreases. Kinetic measurements indicate that during the first 2 h dodecanethiol stays above this critical surface coverage; however, this effect is lost at longer times (see Figure S8 in the supporting information section 5). From the S/Au ratio after 2 h of electrolysis, we can estimate this critical absolute coverage to be 13 %.

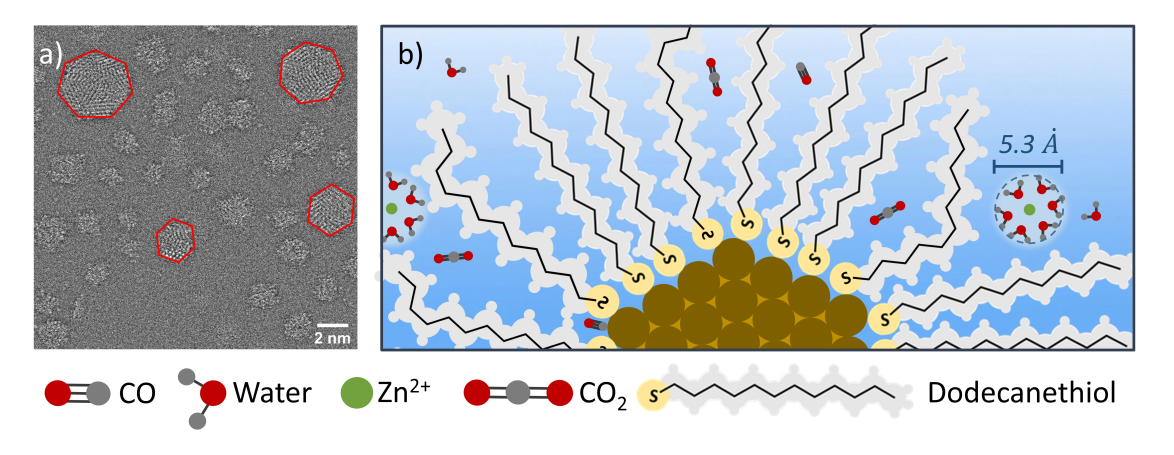


Fig. 5 a) HAADF-STEM images of the DDT-Au nanoparticles with outlines showing the particle geometry. Multiple surface facets can be seen due to the changing grain boundary. b) To scale depiction of an Au nanoparticle (2 nm) with an ordered layer of dodecanethiol surface ligands and solvated  $Zn^{2+}$  ions (5.3 Å). Trace ion deposition on electrocatalysts occurs during  $CO_2R$ , even in pure electrolytes, which decreases Au selectivity for CO. XPS and kinetic measurements show that ordered dodecanethiol capping ligands on Au nanoparticles prevent ion deposition, without blocking  $CO_2R$  active sites.

It is not surprising that the effective dodecanethiol surface coverage from the prespective of a solvated ion would be larger than the absolute surface coverage. The hydrophobic nature of the dodecanethiol will repel the hydrated cations but would not necessarily block CO2, which is similarly hydrophobic. 55,56 In fact, CO<sub>2</sub> is about twice as soluble in dodecane as it is in water. <sup>56,57</sup> This suggests that the dodecanethiol surface ligand would let CO<sub>2</sub> diffuse to the nanoparticle, and may actually serve to concentrate  ${\rm CO}_2$  near the catalyst surface. Consequently, Au edge sites, which are inaccessible to solvated transition metal ions are expected to be readily accessible to CO2. In this study, no effort has been made to optimize this effect by tuning the ligand composition or structure. For example, we expect a correlation between activity and chain length of a linear (or branched) thiol surface ligand based on the competition between mass transport of CO2 and metal ions, and we anticipate that such studies focused on optimization will become the focus of future work.

## 3 Conclusion

We have shown that, despite having a much smaller ECSA, Au nanoparticles passivated with a layer of dodecanethiol have similar activity for CO<sub>2</sub> conversion to CO compared to clean polycrystalline Au as well as Au nanoparticles following ligand removal. Not only does the presence of the dodecanethiol surface ligand not limit CO partial current, we show that these ligand-capped Au nanoparticles are resistant to deactivation under conditions where the Faradic selectivity of polycrystalline Au rapidly decays to zero. We find that although dodecanethiol reductively desorbs from polycrystalline Au, on small Au nanoparticles a fraction of the ligand remains stable for >2 h reaction time at -1.1 V vs RHE. The presence of this surface ligand is shown to significantly limit the deposition of metal ions on the Au nanoparticle catalyst during CO<sub>2</sub>R. These results indicate that dodecanethiol forms a selective membrane on Au nanoparticles, which prevents ion deposition while allowing nearly unhindered transport of CO2. Comparison with other surface ligands and nanoparticles shows that this protecting effect is specific to both the chemical identity and the surface structure of the dodecanethiol monolayer. When operating in an electrolyte obtained from an impure ambient water source, this DDT-Au catalyst produced a CO yield that is more than 100 times greater compared to PC-Au, illustrating that ligand passivation of a nanoparticle surface can greatly benefit catalytic activity despite the loss of ECSA. Given the cost associated with water ultra-purification, this has potential to help address the often overlooked challenge of electrolyte purity that is closely related to the economic viability of CO<sub>2</sub> conversion.

#### 4 Author Information

# **Corresponding Author**

\*Corresponding Author: baker.2364@osu.edu

#### **Author Contributions**

¶ These authors contributed equally.

## Notes

The authors declare no competing financial interest.

# 5 Acknowledgements

Electrochemical catalysis and catalyst pre-and post-reaction characterization was supported by National Science Foundation under under NSF award number 1665280. Nanoparticle synthesis was supported by National Science Foundation under under NSF award number 1503408. XPS was performed at the Ohio State University Surface Analysis Laboratory. Film deposition was performed at the Ohio State University Nanosystems Laboratory. UVO-Au TEM and DDT-Au STEM imaging was performed at the OSU Center for Electron Microscopy and Analysis (CEMAS).

# 6 Supporting Information

The supplementary material contains the details of the 1. Experimental details 2. ECSA 3. Surface coverage calculation by XPS 4. Active site density calculation 5. Stability of DDT on Au nanoparticles 6. XPS of Cu deposition 7. DDT packing structure

8. CO<sub>2</sub>R kinetics in the presence of EDTA 9. Identification of Other products 10. CO<sub>2</sub>R kinetics in ambient water

#### Notes and references

- 1 J. Yu, J. Low, W. Xiao, P. Zhou and M. Jaroniec, *J. Am. Chem. Soc.*, 2014, **136**, 8839–8842.
- W. Luo, X. Nie, M. J. Janik and A. Asthagiri, ACS Catal., 2016,
  6, 219–229.
- 3 J. Pal and T. Pal, Nanoscale, 2015, 7, 14159-14190.
- 4 D. M. Hofmann, D. H. Fairbrother, R. J. Hamers and C. J. Murphy, *ACS Appl. Nano Mater.*, 2019, **2**, 3989–3998.
- 5 D. Gao, H. Zhou, J. Wang, S. Miao, F. Yang, G. Wang, J. Wang and X. Bao, J. Am. Chem. Soc., 2015, 137, 4288–4291.
- 6 S. Liu, H. Tao, L. Zeng, Q. Liu, Z. Xu, Q. Liu and J.-L. Luo, *J. Am. Chem. Soc.*, 2017, **139**, 2160–2163.
- 7 Z. Wu, S. Yang and W. Wu, Nanoscale, 2016, 8, 1237-1259.
- 8 T. Witoon, N. Kachaban, W. Donphai, P. Kidkhunthod, K. Faungnawakij, M. Chareonpanich and J. Limtrakul, *Energy Convers. Manage.*, 2016, **118**, 21–31.
- 9 D. Kim, C. Xie, N. Becknell, Y. Yu, M. Karamad, K. Chan, E. J. Crumlin, J. K. Nørskov and P. Yang, *Journal of the American Chemical Society*, 2017, **139**, 8329–8336.
- L. M. Rossi, J. L. Fiorio, M. A. Garcia and C. P. Ferraz, *Dalton Trans.*, 2018, 47, 5889–5915.
- 11 L. Altmann, S. Kunz and M. Baumer, *J. Phys. Chem. C*, 2014, **118**, 8925–8932.
- 12 J. R. Pankhurst, Y. T. Guntern, M. Mensi and R. Buonsanti, *Chemical science*, 2019, **10**, 10356–10365.
- 13 C. Kim, T. Eom, M. S. Jee, H. Jung, H. Kim, B. K. Min and Y. J. Hwang, *ACS Catal.*, 2017, **7**, 779–785.
- 14 J. A. Trindell, J. Clausmeyer and R. M. Crooks, *J. Am. Chem. Soc.*, 2017, **139**, 16161–16167.
- 15 S. Jeong, G.-M. Kim, G.-S. Kang, C. Kim, H. Lee, W.-J. Kim, Y. K. Lee, S. Lee, H. Kim, H. K. Lim et al., The Journal of Physical Chemistry C, 2019, 123, 29184–29191.
- 16 Z. Cai, Y. Zhang, Y. Zhao, Y. Wu, W. Xu, X. Wen, Y. Zhong, Y. Zhang, W. Liu, H. Wang et al., Nano Research, 2019, 12, 345–349.
- 17 H. Shang, T. Wang, J. Pei, Z. Jiang, D. Zhou, Y. Wang, H. Li, J. Dong, Z. Zhuang, W. Chen et al., Angewandte Chemie International Edition, 2020.
- 18 Z. Wang, L. Wu, K. Sun, T. Chen, Z. Jiang, T. Cheng and W. A. Goddard III, *The journal of physical chemistry letters*, 2018, 9, 3057–3061.
- 19 T. Taguchi, K. Isozaki and K. Miki, *Adv. Mater.*, 2012, **24**, 6462–6467.
- 20 I. Schrader, J. Warneke, J. Bakenkohler and S. Kunz, *J. Am. Chem. Soc.*, 2015, **137**, 905–912.
- 21 M. Moreno, F. J. Ibanez, J. B. Jasinski and F. P. Zamborini, *J. Am. Chem. Soc.*, 2011, **133**, 4389–4397.
- 22 S. Campisi, D. Ferri, A. Villa, W. Wang, D. Wang, O. Krocher and L. Prati, *J. Phys. Chem. C*, 2016, **120**, 14027–14033.
- 23 P. Liu, R. Qin, G. Fu and N. Zheng, J. Am. Chem. Soc., 2017, 139, 2122–2131.

- 24 A. Villa, D. Wang, G. M. Veith, F. Vindigni and L. Prati, *Catal.*: *Sci. Technol.*, 2013, 3, 3036–3041.
- 25 B. Wu, H. Huang, J. Yang, N. Zheng and G. Fu, Angew. Chem., Int. Ed., 2012, 51, 3440–3443.
- 26 R. K. Grasselli and A. Sleight, *Structure-activity and selectivity relationships in heterogeneous catalysis*, Elsevier, 1991.
- 27 T. Ressler, R. E. Jentoft, J. Wienold, F. Girgsdies, T. Neisius and O. Timpe, *Nucl. Instrum. Methods Phys. Res., Sect. B*, 2003, **200**, 165–170.
- 28 N. Todoroki, H. Tei, H. Tsurumaki, T. Miyakawa, T. Inoue and T. Wadayama, *ACS Catal.*, 2019, **9**, 1383–1388.
- 29 S. Mezzavilla, S. Horch, I. E. Stephens, B. Seger and I. Chorkendorff, *Angew. Chem.*, 2019, **131**, 3814–3818.
- 30 W. Zhu, R. Michalsky, O. Metin, H. Lv, S. Guo, C. J. Wright, X. Sun, A. A. Peterson and S. Sun, *J. Am. Chem. Soc.*, 2013, 135, 16833–16836.
- 31 W. Zhang, J. He, S. Liu, W. Niu, P. Liu, Y. Zhao, F. Pang, W. Xi, M. Chen, W. Zhang *et al.*, *Nanoscale*, 2018, **10**, 8372–8376.
- 32 S. Back, M. S. Yeom and Y. Jung, ACS Catal., 2015, **5**, 5089–5096.
- 33 W. Zhu, Y.-J. Zhang, H. Zhang, H. Lv, Q. Li, R. Michalsky, A. A. Peterson and S. Sun, *J. Am. Chem. Soc.*, 2014, **136**, 16132–16135.
- 34 Y. i. Hori, *Modern aspects of electrochemistry*, Springer, 2008, pp. 89–189.
- 35 Y. Hori, H. Konishi and T. Futamura, *Electrochim. Acta*, 2005, **50**, 5354–5369.
- 36 J. Clavilier, J. Feliu and A. Aldaz, *Journal of electroanalytical chemistry and interfacial electrochemistry*, 1988, **243**, 419–433.
- 37 G. Klusewitz and J. Viegh, 13th Annual IEEE/SEMI Advanced Semiconductor Manufacturing Conference. Advancing the Science and Technology of Semiconductor Manufacturing. ASMC 2002, 2002, pp. 340–346.
- 38 A. Bennett, Filtr. Separat., 2006, 43, 28-32.
- 39 A. Wuttig and Y. Surendranath, ACS Catalysis, 2015, 5, 4479– 4484.
- 40 C. G. Worley and R. W. Linton, *J. Vac. Sci. Technol.*, *A*, 1995, 13, 2281–2284.
- 41 M. J. Hostetler, J. E. Wingate, C.-J. Zhong, J. E. Harris, R. W. Vachet, M. R. Clark, J. D. Londono, S. J. Green, J. J. Stokes, G. D. Wignall *et al.*, *Langmuir*, 1998, 14, 17–30.
- 42 D.-F. Yang, C. Wilde and M. Morin, *Langmuir*, 1997, **13**, 243–249
- 43 M. M. Walczak, D. D. Popenoe, R. S. Deinhammer, B. D. Lamp, C. Chung and M. D. Porter, *Langmuir*, 1991, 7, 2687–2693.
- 44 D. Tsai, R. Zangmeister, L. Pease Iii, M. Tarlov and M. Zachariah, *Langmuir*, 2008, **24**, 8483–8490.
- 45 Y. Cheng, S. Lu, W. Xu, H. Wen and J. Wang, *J. Mat. Chem. A*, 2015, **3**, 16774–16784.
- 46 S. Ringe, C. G. Morales-Guio, L. D. Chen, M. Fields, T. F. Jaramillo, C. Hahn and K. Chan, *Nat. Commun.*, 2020, 11, 1–11.
- 47 B. A. Zhang, T. Ozel, J. S. Elias, C. Costentin and D. G. Nocera,

- ACS Cent. Sci., 2019, 5, 1097-1105.
- 48 D. Kim, J. Resasco, Y. Yu, A. M. Asiri and P. Yang, *Nat. Commun.*, 2014, **5**, 1–8.
- 49 Y. Chen, C. W. Li and M. W. Kanan, *J. Am. Chem. Soc.*, 2012, **134**, 19969–19972.
- 50 Z. Qi, J. Biener and M. Biener, *ACS Appl. Energy Mater.*, 2019, **2**, 7717–7721.
- 51 A. N. Bordenyuk, C. Weeraman, A. Yatawara, H. D. Jayathilake, I. Stiopkin, Y. Liu and A. V. Benderskii, *J. Phys. Chem. C*, 2007, **111**, 8925–8933.
- 52 R. Reske, H. Mistry, F. Behafarid, B. Roldan Cuenya and P. Strasser, *J. Am. Chem. Soc.*, 2014, **136**, 6978–6986.
- 53 O. E. D. of Surface Water, Biological and water quality study of the Olentangy River and selected tributaries 1999: Delaware and Franklin Counties, Ohio, Ohio EPA, 2001.
- 54 N. Larsen, H. Biebuyck, E. Delamarche and B. Michel, *J. Am. Chem. Soc.*, 1997, **119**, 3017–3026.
- 55 D. Lide, CRC Press, 2007, 88, pp 99–100.
- 56 P. G. Fogg, Carbon Dioxide in non-aqueous solvents at pressures less than 200 kPa, Elsevier, 2017, vol. 50, pp. 19–27.
- 57 J. J. Carroll, J. D. Slupsky and A. E. Mather, *J. Phys. Chem. Ref. Data*, 1991, **20**, 1201–1209.